



Published in final edited form as:

Clin Cancer Res. 2009 May 15; 15(10): 3277–3286. doi:10.1158/1078-0432.CCR-08-2502.

IMMUNE-DEFICIENT MOUSE STRAINS DISPLAY MARKED VARIABILITY IN GROWTH OF HUMAN MELANOMA LUNG METASTASES

Beatriz M. Carreno¹, Joel R. Garbow^{5,6}, Grant R. Kolar³, Erin N. Jackson⁴, John A. Engelbach⁵, Michelle Becker-Hapak¹, Leonidas N. Carayannopoulos¹, David Piwnica-Worms^{2,4,6}, and Gerald P. Linette¹

¹Department of Medicine, Washington University School of Medicine, St Louis, MO 63110

²Department of Developmental Biology, Washington University School of Medicine, St Louis, MO 63110

³Department of Pathology-Immunology, Washington University School of Medicine, St Louis, MO 63110

⁴Molecular Imaging Center, Washington University School of Medicine, St Louis, MO 63110

⁵Biomedical Magnetic Resonance Laboratory, Mallinckrodt Institute of Radiology, Washington University School of Medicine, St Louis, MO 63110

⁶Siteman Cancer Center, Washington University School of Medicine, St Louis, MO 63110

Abstract

Purpose—Immune-deficient mice serve as critical hosts for transplantation of xenogeneic cells for *in vivo* analysis of various biological processes. Since investigators typically select one or two immune-deficient mouse strains as recipients, no comprehensive study has been published documenting differences in human tumor engraftment. Taking advantage of the increased metastatic potential of RhoC-expressing human (A375) melanoma cells, we evaluate 4 immune-deficient mouse strains: *scid*, NOD-*scid*, NOD-*scid* $\beta 2m^{\text{null}}$, and NOD-*scid* $IL2R\gamma^{\text{null}}$ as xenograft tumor recipients.

Experimental design—Bioluminescence, magnetic resonance imaging and histopathology was employed to monitor serial tumor growth. NK cell function was examined in each mouse strain using standard ⁵¹Chromium release assays.

Results—Melanoma metastases growth is delayed and variable in *scid*, and NOD-*scid* mice. In contrast, NOD-*scid* $\beta 2m^{\text{null}}$ and NOD-*scid* $IL2R\gamma^{\text{null}}$ mice show rapid tumor engraftment, although tumor growth is variable in NOD-*scid* $\beta 2m^{\text{null}}$ mice. NK cells were detected in all strains except NOD-*scid* $IL2R\gamma^{\text{null}}$, and *in vitro* activated *scid*, NOD-*scid* and NOD-*scid* $\beta 2m^{\text{null}}$ NK cells kill human melanoma lines and primary melanoma cells. Expression of human NKG2D ligands MHC

Corresponding Author: Beatriz M. Carreno, Washington University School of Medicine, Division of Oncology, 660 South Euclid Avenue, Campus Box 8007, St Louis, MO 63110. Phone: 314-362-9407, Fax: 314-362-9333, E-mail: E-mail: bcarreno@wustl.edu.

TRANSLATIONAL RELEVANCE

Immune-deficient mice are widely used in cancer research to study human cancer biology and evaluate new therapeutics. Although the athymic nude mouse has served as the standard recipient for over 40 years, new immune-deficient mouse strains have been developed that possess well defined defects in adaptive and innate immunity. In this report, we examined the influence of residual innate immunity on the development of pulmonary metastases using the human A375-RhoC melanoma. The integration of small animal imaging with a clinically relevant lung metastases model reveals the inherent variability among the *scid*, NOD-*scid*, and NOD-*scid* $\beta 2m^{\text{null}}$ strains. Genetic ablation of the $IL2R\gamma$ chain leads to an absolute NK deficiency in the NOD-*scid* $IL2R\gamma^{\text{null}}$ strain and results in consistent engraftment of human melanoma. Our observation expands the potential to study human melanoma and establishes a new standard to evaluate novel agents in a clinically relevant animal model.

class I chain-related A and B molecules renders melanoma susceptible to murine NK cell-mediated cytotoxicity and killing is inhibited by antibody blockade of murine NKG2D.

Conclusions—Murine NKG2D recognition of MICA/B is an important receptor-ligand interaction employed by NK cells in immune-deficient strains to limit engraftment of human tumors. The absolute NK deficiency in NOD-*scid* *IL2R γ* ^{null} animals makes this strain an excellent recipient of melanoma and potentially other human malignancies.

INTRODUCTION

Mouse models of human cancer serve as essential experimental systems and genetically defined immune-deficient mouse strains constitute a valuable tool for studying tumorigenesis. Athymic (nude) mice have been the standard for establishing *in vivo* models of human malignancies (1). However, the presence of residual adaptive and innate immunity can interfere with the establishment of tumor xenografts. Athymic mice develop small numbers of mature $\alpha\beta$ TCR lymphocytes with age; in addition, robust NK cell activity is present and increases with age (2,3). Numerous reports confirm variable rates of human tumor growth in athymic animals (4-6); for example, of 200 human breast cancer samples tested in nude mice, just 25 (12.5%) grew as xenografts at the site of subcutaneous implantation (7). Severe combined immunodeficiency (*scid*) mice have relative B and T cell deficiencies and are often used as recipients of human xenografts. Improved tumor engraftment rates have been reported in the NOD-*scid* strain, where introduction of the *scid* mutation into the non-obese diabetic (NOD) background results in reduced macrophage and NK function, as well as, an absence of complement-dependent hemolytic activity (8,9). Recently, two additional immune-deficient strains have been described: NOD-*scid* $\beta 2m$ ^{null}, and NOD-*scid* *IL2R γ* ^{null} (10). The NOD-*scid* $\beta 2m$ ^{null} strain was developed by backcrossing the $\beta 2m$ ^{null} mutation to the NOD-*scid* strain resulting in mice deficient in MHC class I expression (NOD-*scid* $\beta 2m$ ^{null}). Accumulating data suggest that NK cells that develop in a MHC class I deficient background are unlicensed and hence, unable to kill susceptible targets upon activation (11). The NOD-*scid* *IL2R γ* ^{null} strain was developed by introduction of the *IL2R γ* ^{null} mutation into the NOD-*scid* strain (12). Absence of *IL2R γ* , the common cytokine-receptor γ -chain shared by the IL-2, IL-4, IL-7, IL-9, IL-15 and IL-21 receptors, leads to impaired NK cell development due to absence of IL-15 signaling (13). Improved engraftment of human cord blood CD34+ cells has been reported in NOD-*scid* $\beta 2m$ ^{null} and NOD-*scid* *IL2R γ* ^{null} highlighting the potential use of these strains as recipients of tumor xenografts (14).

Animal models of human melanoma are limited. Clark et al. (15), generated highly metastatic human melanoma (A375) cells through *in vivo* selection of lung metastasis in nude mice. A genomic analysis of metastatic A375 variants demonstrated that RhoC, a RAS-related guanosine triphosphatase, is an important determinant of tumor cell invasion. Further studies have shown that RhoC plays a role in cytoskeleton organization and is essential for tumor metastasis (16). In a recent series of studies, Beige-*scid* mice were employed to evaluate therapeutics for human melanoma A375-RhoC pulmonary metastasis (17,18). However, NK cell function was not studied and since no other mouse strains were evaluated, the relative impact of residual innate immunity remains undefined in the A375-RhoC model.

In the present study, we evaluate human melanoma (A375-RhoC) pulmonary metastases in four immune-deficient mouse strains: *scid*, NOD-*scid*, NOD-*scid* $\beta 2m$ ^{null}, and NOD-*scid* *IL2R γ* ^{null} strains. Tumor growth was monitored non-invasively by imaging using bioluminescence (BLI) and magnetic resonance imaging (MRI) combined with histopathological assessment. BLI allowed for accurate, real time serial *in vivo* quantitation of tumor burden, while MRI permitted three-dimensional structural imaging of tumor. Our results show that NOD-*scid* *IL2R γ* ^{null} mice are highly permissive for engraftment of human melanoma

metastases, while endogenous NK activity in the other three strains delayed or, in certain instances, completely prevented the formation of pulmonary metastasis. Importantly, we demonstrate that expression of human NKG2D ligands MHC class I chain-related A (MICA) and B (MICB) molecules by melanoma confers susceptibility to murine NK-mediated cytotoxicity.

MATERIALS and METHODS

Mouse strains

CB17-*Prkdc^{scid}/J* (*scid*), NOD.CB17-*Prkdc^{scid}/J* (NOD-*scid*), NOD.Cg-*Prkdc^{scid}* *B2m^{tm1Unc}/J* (NOD-*scid* *β2m^{null}*), and NOD.Cg-*Prkdc^{scid}* *IL2rγ^{tm1Wjll}/SzJ* (NOD-*scid* *IL2Rγ^{null}*) mice were obtained from Jackson Laboratories (Bar Harbor, ME) and bred and housed according to the guidelines of Washington University, Division of Comparative Medicine. Strain background is Balb/c (H-2^d) for *scid* and NOD (H-2^{g7}) for all other strains. The animal ethics committee approved all experiments. All mice used were between 7 and 14 weeks of age.

Melanoma cell lines

The human melanoma cell line A375P-RhoC-*GFP* (15) was transduced with a retrovirus expressing a click beetle red luciferase (*cbr-luc*)/enhanced yellow fluorescence protein (eYFP) fusion gene. A stable cell line was selected by flow cytometry on a MoFlo (Dako, Carpinteria, CA) sorting for cells expressing high *GFP* (for RhoC expression) and eYFP (for *cbr-luc* expression) levels. Stable A375 RhoC-luciferase expressing cell line is referred to as A375RC-Luc. Human melanoma lines DM6 and LoX (ATCC) are previously described (19). CG mel is a primary human melanoma (S100+ HMB45+) generated in our laboratory from a resected lymph node metastases. DM6, LoX and CG lines stably expressing high *GFP* (for RhoC expression) and eYFP (for *cbr-luc* expression) levels were generated as described above for A375. M14 melanoma cells (20) were transfected with MICA and MICB cDNA (21) using lipofectamine as directed by manufacturer's instructions (Invitrogen, Carlsbad, CA). Clones were selected using G418 at 1mg/ml and stable expression of MICA and MICB confirmed by flow cytometry using anti-MICA/B mAb 6D4 (22) (Biolegend, San Diego, CA). Expression of ULBP1-3 by melanoma cell lines was determined by flow cytometry using antibodies (23) obtained from Axxora (San Diego, CA).

In vivo imaging

For serial analysis of tumor growth, mice were injected intravenously with 2.5×10^6 RhoC/luciferase-expressing tumor cells in 200 μ l PBS. After tumor inoculation (2-3 h), mice were injected intraperitoneally with 150 mg/kg D-luciferin (Biosynth, Naperville, IL)/ PBS and imaged 10 minutes later. Imaging was performed using a charge-coupled device (CCD) camera (IVIS 50; Caliper Corporation; exposure time 1-30 seconds, binning 8, field of view 12, f/stop 1, open filter) at the Molecular Imaging Center (Washington University, St. Louis) as described previously (24). Mice were anesthetized using isoflourane (2.5 % vaporized in O₂). For analysis, total photon flux (photons per second) was measured from a fixed region of interest (ROI) over the thorax/liver area using Living Image 2.50 and IgorPro software (Wavemetrics, Portland, OR) (24). Animals were monitored bi-weekly for health and signs of tachypnea and weight loss. MRI experiments were performed in the Biomedical MR Laboratory (Washington University, St. Louis) as previously described (25,26). Briefly, respiratory gated, spin-echo MR images were collected in a 4.7 T Oxford magnet (Oxford, UK) interfaced with a Varian NMR Systems (Palo Alto, CA) INOVA console. Animals were anesthetized with isoflourane (1% v/v in O₂) and animal core body temperature was maintained at $37 \pm 1^\circ\text{C}$ by circulation of warm air through the bore of the magnet. Synchronization of MR data collection with animal respiration was achieved with a home-built respiratory-gating unit (27) and all images were

collected during post-expiratory periods. Imaging parameters were TR=3 s, TE=20 ms, 2.5 cm FOV, slice thickness = 0.5 mm. BLI was performed weekly; MRI experiments were performed at selected time points as described.

Histopathology

After MRI on day 28 (for NOD-*scid* *IL2R γ ^{null}*) or day 35 (all other strains), animals were sacrificed, lungs excised, and fixed in 10% formalin overnight. Paraffin-embedded tissues were sectioned and stained by hematoxylin-eosin. Tissues were examined in a blinded manner, at least 5 sections of tumor were examined by a pathologist. Two animals per strain were evaluated. Representative slides from each animal were scanned with modified 35 millimeter slide scanner, areas of tumor quantified and expressed as a percentage of total lung tissue using NIH Image Software (NIH, Bethesda, MD).

Immunologic assays

Spleen cell suspensions were prepared and stained using anti-CD3, anti-CD45.1, anti-CD49b-PE (DX5) and/or anti-NKG2D-biotin (28). Antibodies were obtained from eBioscience or Biologend (San Diego, CA). Cells were incubated with anti-CD32/CD16 for 5 min at 4°C, followed by specific antibodies, washed, and in the case of anti-NKG2D biotin followed by SA-APC. Staining with murine NKG2D and control tetramer was performed as described (29). Multiparameter flow cytometry analysis was performed using a B-D Biosciences FACScan flow cytometer modified with a second, 633 nm 25 mW laser, and two additional detectors with bandwidths at 660 nm and 760 nm. For assessment of NK function, spleen cell suspensions were depleted of red blood cells and cultured at 2×10^6 cells/ml in 24 well tissue culture plates for 48 h in RPMI/10% FCS/ 2 mM glutamine, HEPES, Pen-Strep, murine IL-15 (100 ng/ml, Peprotec, Rock Hill, NJ) and murine IL-18 (100 ng/ml, R&D Systems, Minneapolis, MN). For ^{51}Cr -release assays, target cells (10^6 cells/ml) were labeled with 1 μM ^{51}Cr for 1 h, washed and added to spleen cultures at various E:T ratios and incubated in triplicate for an additional 4 h. ^{51}Cr -release was quantitated in a Tri-Lux Wallac as described (30).

Statistical Analysis

Unpaired t-test was performed to evaluate tumor growth kinetics among strains and the differences were significant if p value <0.05. The Inter-quartile range were determined to evaluate tumor growth variability among strains and Kaplan-Meier product-limit method was used to calculate survival rates; differences between groups were determined using log rank analysis; p values <0.05 indicate significance in survival rates. Repeated measure one way ANOVA was performed to evaluate lysis of melanoma by NK cells; for pairwise comparison a Tukey's test was performed post ANOVA analysis. All analysis was performed using Prism version 5 (GraphPad Software Inc., San Diego, CA)

RESULTS

Human melanoma pulmonary metastases show different rates of engraftment in immune-deficient mouse strains

Human melanoma cells expressing RhoC (A375-RhoC) exhibit lung tropism after intravenous transplantation in athymic mice (15). To evaluate the impact of residual murine innate immunity on the development of human melanoma pulmonary metastases, we assessed A375-RhoC growth in *scid*, NOD-*scid* (NS), NOD-*scid* $\beta 2m^{\text{null}}$ (NSB), and NOD-*scid* *IL2R γ ^{null}* (NSG). Bioluminescence and MRI imaging modalities were employed to monitor rates of tumor engraftment (25,31). A375-RhoC cells stably expressing a luciferase reporter (A375RC-Luc, 2.5×10^6) were administered intravenously on day 0 and animals were examined using

BLI 2-3 h after tumor inoculation and weekly thereafter to assess the kinetics of tumor growth (31). Serial BLI images of one representative mouse per strain are shown in Figure 1A. Tumor growth as assessed by BLI signal intensity is most rapid in NSG animals followed by the NSB strain (Figure 1B). The growth of melanoma lung metastasis was delayed in *scid* and NS mice when compared to NSG and NSB (Figures 1B). The mean time to reach a photon flux of 1×10^9 photon/sec was: *scid*, 31d; NS, 28d; NSB, 14d and NSG, 8d (Figure 1B). As tissue attenuation of BLI signal is fixed at any given depth, different times to reach equivalent BLI signals are likely to reflect distinct tumor growth kinetics among strains. Tumor growth was confined to the lung in all strains as no BLI signal was detected outside this organ (Figure 1A). Imaging results were verified by necropsy on day 28-35 (data not shown).

To further characterize tumor growth and correlate BLI with anatomy, MRI was performed on 2 animals per strain. Coronal, respiratory-gated spin-echo images of a representative mouse per strain (day 28 for NSG; day 35 all other strains) are shown together with histopathology of lung tissue (hematoxylin and eosin stained sections) (Figure 1C). Two views, 10X and 100X of lung tissue sections are shown for comparison. Based on total lung parenchyma, quantitative tumor burden for each strain (n=2 mice per strain) was assessed microscopically in a blinded manner: *scid*, 7%; NS, 35%; NSB, 62% and NSG, 95%. MRI detection of pulmonary metastases is less sensitive than BLI; in *scid* mice, BLI shows clear signal on day 35 though no solid tumor is detected by MRI. In contrast, innumerable pulmonary metastases are visualized in both NSB and NSG strains (Figure 1C, **right column**). Although several lung nodules are evident in the NS animals; the tumor burden is substantially less and is consistent with the BLI results.

Human melanoma shows variable engraftment in NOD-*scid* $\beta 2m^{null}$

We performed additional experiments to further characterize the kinetics of tumor growth in the 3 most permissive strains: NS, NSB and NSG. Figure 2A-C shows a summary of tumor growth rates as determined by BLI for individual animals at weekly time points. BLI signal is reproducibly detected in all animals within 2-3 h after i.v. injection of A375RC-luc cells. In spite of brisk tumor growth in both NSB and NSG, tumor engraftment is highly variable in NSB as shown by the larger inter-quartile range among mice in the NSB strain (Figure 2B). Between day 28 and 35, 60% of NSG mice died due to tumor progression. In contrast, no deaths were seen prior to day 35 in any tumor-bearing NS and NSB animal; NS mice show significantly delayed tumor growth compared to NSB and NSG mice. Survival curves of NSB and NSG in a representative experiment (n=10 mice per cohort) are shown in Figure 2D. The median survival was 42 days for NSB and 32 days for NSG; in contrast, all NS mice survived past 48 days (data not shown).

Rapid engraftment of multiple human melanoma lines in NOD-*scid* $IL2R\gamma^{null}$ (NSG) mice

Due to the consistent and reproducible growth of A375RC-luc observed in NSG, we selected this mouse strain to evaluate the growth of three additional Rho-C/luciferase expressing human melanoma cell lines. DM6 (19) and Lox are well characterized cell lines while CG mel is a primary (low passage) melanoma line isolated in our laboratory. NS mice (strain background NOD: H-2^{g7}) were used as the comparator strain with NSG mice as these strains share identical genetic background (10). Average BLI values for mice (n=3) at each time point is shown in Figure 3A-D. Each melanoma studied exhibited a distinct rate and level of engraftment in NS and NSG mice as assessed by BLI. Rates and levels of engraftment of A375, Lox and CG were higher in NSG relative to NS mice. Interestingly, despite similar BLI signal at day 0 in DM6-bearing NS and NSG, no BLI signal was detected after day 7 in NS mice suggesting complete rejection of DM6 in this strain. In agreement with this finding, no evidence of tumor was observed upon autopsy of DM6-bearing NS lungs (day 50 after tumor inoculation, data not

shown). Altogether, these results demonstrate that NSG mice are a permissive host for engraftment of human melanoma pulmonary metastasis.

NK characterization and function in immune-deficient strains

The superior engraftment of human melanoma in NSG, a strain devoid of NK cells, implicated murine NK cells as the effector population responsible for tumor rejection. Flow cytometry analysis confirms the presence of NK cells in *scid* (48.9%), NS (27.3%) and NSB (30.5%) spleen CD45⁺ populations as determined by the co-expression of CD49b (DX5) and NKG2D. No reactivity of NSG spleen cells was observed with anti-CD49b or anti-NKG2D indicating that NK cells were absent in this mouse strain as previously noted (13) (Figure 4A and B).

To assess NK effector function, spleen cells from the various strains were activated *in vitro* with IL-15 + IL-18 and 48 h later assessed for their capacity to recognize human melanoma cells as targets in a ⁵¹Cr-release assay. NSG spleen cells cultured in IL-15 + IL-18 yielded no appreciable numbers of NK cells and displayed no killing against human melanoma or YAC cells confirming the complete absence of NK cells in this strain (data not shown). IL-15 + IL-18-activated *scid*, NS and NSB spleen cells were able to recognize and kill YAC cells (data not shown), as well as, multiple human melanoma lines (Figure 4C). These findings indicate that murine NK cells from selected immune-deficient mice have the ability to recognize human melanoma.

Expression of NKG2D ligands MICA, MICB and ULBP1-3 by human melanoma

MHC class-I chain related A and B (MICA and MICB) and UL-16 binding proteins (ULBP) 1-3 are the human ligands for NKG2D, a NK activating receptor (32). Several reports provide evidence that murine NKG2D can bind human NKG2D ligands such as MICB, ULBP-1 and ULBP-2 (33,34). To further investigate the mechanism of murine NK recognition of human melanoma, we determined the expression of NKG2D ligands on selected melanoma cell lines, including M17 a melanoma cell line obtained from the European Searchable Tumor Cell Line and Data Bank (ESTDAB) and reported as MICA/B negative (35). As shown in Figure 5A, ULBP 1, 2 and 3 expression among melanoma cell lines was heterogeneous. Most lines were negative for ULBP-1, and expressed variable levels of ULBP-2 and ULBP-3. Only one cell line, DM6, expressed all three ULBP molecules. No correlation was observed between ULBP expression and the ability of murine NK cells to recognize human melanoma. In contrast, seven of nine melanoma cell lines expressed MICA/B as detected by the 6D4 mAb (22). Interestingly, low levels of MICA/B expression in M14 and M17 cells correlated with low susceptibility to murine NK cell cytotoxicity (Figures 5A-B, 6A) suggesting a potential role for MICA/B in murine NK cytotoxicity against human melanoma cells.

MICA and B expression by human melanoma confers susceptibility to murine NKG2D mediated cytotoxicity

To investigate MICA/B - murine NKG2D interactions and its functional consequences, M14 cells were transfected with MICA or MICB and evaluated for binding of murine (mu)NKG2D tetramer (29). As shown in Figure 5B, M14 cells show no reactivity with MICA/B mAb and exhibit low levels of muNKG2D tetramer binding. This finding is consistent with low level expression of ULBP-2 by M14 since mu NKG2D tetramer can bind ULBP-2 as shown by Sutherland et al. (34). M14 cells were transfected with cDNA encoding MICA or MICB and expression was confirmed using the 6D4 mAb. Moreover, expression of MICA and MICB in M14 cells results in increased binding of mu NKG2D tetramer as shown in Figure 5B. In cytotoxicity assays, neither M17 nor M14 were susceptible to lysis by activated NK cells (Figure 6A), while A375 and DM6 were killed in a dose-dependent manner at the indicated E:T ratios. Expression of MICA and MICB rendered M14 cells sensitive to murine NK lysis as demonstrated at multiple E:T ratios (Figure 6B) compared to control M14 cells. In multiple

independent experiments (n=6), the expression of either MICA or MICB was sufficient to render M14 melanoma sensitive to NOD-*scid* NK cell lysis (Figure 6C). The involvement of murine NKG2D receptor in melanoma recognition was examined using the antagonistic anti-NKG2D mAb C7 (28). Pre-treatment of activated NK cells with anti-NKG2D mAb resulted in a significant decrease in MICA and MICB recognition with no statistically significant effect on control M14 cells (Figure 6D). Altogether, these data support the finding that MICA and MICB are capable of binding to and activating murine NK cells through interaction with their NKG2D receptor.

DISCUSSION

In the present study, we compared *scid*, NOD-*scid*, NOD-*scid*- $\beta 2m^{null}$ and NOD-*scid* $IL2R\gamma^{null}$ mice as recipients for human melanoma. Engraftment of human melanoma pulmonary metastasis in NOD-*scid* $IL2R\gamma^{null}$ mice is brisk and reproducible relative to the other strains examined. Despite multiple attempts to isolate and grow NK cells from NOD-*scid* $IL2R\gamma^{null}$ mice, we were unsuccessful and thus, confirm the original observation that ablation of the common cytokine-receptor γ -chain ($IL2R\gamma$) confers an absolute NK cell deficiency (13). Our results also suggest that murine NK cells utilize NKG2D to recognize MICA/B and we propose that this mechanism accounts for the increased xenograft rejection observed in *scid*, NOD-*scid*, NOD-*scid*- $\beta 2m^{null}$ mice.

We initially observed dramatic differences in human melanoma engraftment among NOD-*scid* $\beta 2m^{null}$ littermates and were perplexed by this inconsistency. Although NK cells from NOD-*scid* $\beta 2m^{null}$ mice are present in similar percentages as *scid* and NOD-*scid* animals, it appears that NK cells which develop in a MHC class I deficient environment are functionally impaired (11,36). However, our findings suggest the presence of residual/partial NK cell activity in NOD-*scid* $\beta 2m^{null}$ mice since some animals clearly have delayed tumor engraftment (Figure 2B). The variable engraftment rates of human CD34+ stem cells in NOD-*scid* $\beta 2m^{null}$ animals supports this conclusion (37). In support of NK cells retarding the growth of xenografts, administration of anti-CD122 antibody to deplete endogenous NK cells in NOD-*scid* mice has been shown to improve engraftment of human hematopoietic stem cells (38) as well as solid tumor stem cells (39). The inconsistent tumor growth seen is likely to reflect variable levels of NK function among mouse strains and not heterogeneity in tumor sample as similar results were obtained using tumor lines or clones obtained by limiting dilution (data not shown). The inherent advantage of using the NOD-*scid* $IL2R\gamma^{null}$ strain is that gene ablation of the $IL2R\gamma$ chain leads to absolute NK deficiency (12,13) and results in remarkable consistency of human melanoma engraftment (this study). Additionally, NOD-*scid* $IL2R\gamma^{null}$ do not develop thymic lymphoma with age, thus allowing for long-term studies in these mice. In contrast, NOD-*scid* and NOD-*scid* $\beta 2m^{null}$ animals have a high incidence of thymic lymphomas which are fatal (10).

NK function is regulated by inhibitory and activating cell surface receptors (40). NKG2D, a C-type lectin-like molecule, is a major NK activating receptor that interacts with a diverse array of ligands (41,42). NKG2D ligands include retinoic acid early transcript 1 (RAE1) proteins and minor histocompatibility protein H60 and MULTI in mice and MICA, MICB and ULBPs in human (32). Recent data in both NKG2D deficient mice and gain of function studies using a novel chimeric NKG2D construct support the critical role of NKG2D in tumor surveillance (43,44). Human melanomas and various carcinomas have been reported to express MICA/B and/or ULBPs and both ligands have been shown to be involved in human NK recognition of tumors (20,45). Interestingly, NKG2D from one species can bind ligands from another; for example murine NKG2D has been previously shown to bind human ligands MICB, ULBP-1 and ULBP-2 (33,34). Several previous studies have examined NK cell function in NOD mice and shown some degree of impairment in target cell recognition (compared to the C57BL/6

strain)(46,47), however, little direct information regarding NOD-*scid* NK cell function in the context of xenograft recognition is available. Our results demonstrate that MICA/B - murine NKG2D interaction leads to recognition of human melanoma which may, in turn, result in decreased tumor engraftment in certain immune-deficient strains. The beige-*scid* mouse has also been reported to be permissive to human melanoma xenografts and as shown by Elsner and colleagues, MICA/B appears to be the tumor associated rejection ligand recognized by murine NKG2D. (48). Interestingly, beige-*scid* mice have large numbers of DX5+ NK cells that express low levels of NKG2D (data not shown). Thus, our results are consistent with the observation that NKG2D recognition of MICA/B and ULBPs may prevent/delay engraftment of many human solid tumors in immune-deficient mouse strains.

Small animal imaging provides significant advantages to monitor tumor growth in experimental models (49). Whole body bioluminescence imaging with luciferase reporters is remarkably sensitive, facile to execute, serially and allows detection of early metastases in various tissues. MRI is less sensitive but has inherent advantages including superior spatial resolution and no requirement for reporter constructs. A recent report evaluating positron-emission tomography, X-ray computed tomography, and BLI imaging modalities documents the ability for detecting human melanoma lung metastases (A375-M) in *scid* mice at day 45 (50). In our model, ¹⁸F-FDG-PET imaging was performed on several animals which could, in fact, detect A375-RhoC lung metastases as early as day 30 (data not shown).

In summary, our study highlights murine NKG2D recognition of MICA/B as an important receptor-ligand interaction employed by NK cells in immune-deficient strains to limit engraftment of human tumors. Since NOD-*scid* *IL2R γ ^{null}* mice have an absolute NK cell deficiency as well as additional innate and adaptive defects, this strain appears to be the best recipient for human melanoma.

ACKNOWLEDGMENTS

We thank Richard Hynes, John DiPersio, Timothy Graubert, Marco Colonna and Thomas Spies for reagents; Julie Ritchey and Matthew Holt for excellent technical assistance; Siteman Cancer Center High Speed Cell Sorter Core and Small Animal Cancer Imaging Core facilities for expert assistance. We thank Wayne Yokoyama and Todd Fehniger for advice. Financial support: ACS IRG-58-010-49 (G.L), NIH P50 CA94056 (D.P-W), NIH/NCI R24 CA 83060 and NCI P30 CA91842 (J.G.), NIH/NIAID K08 AI57361 (L.N.C).

Abbreviations

NS, NOD-*scid*; NSB, NOD-*scid* $\beta 2m^{\text{null}}$; NSG, NOD-*scid* *IL2R γ ^{null}*; BLI, bioluminescence; MRI, magnetic resonance imaging.

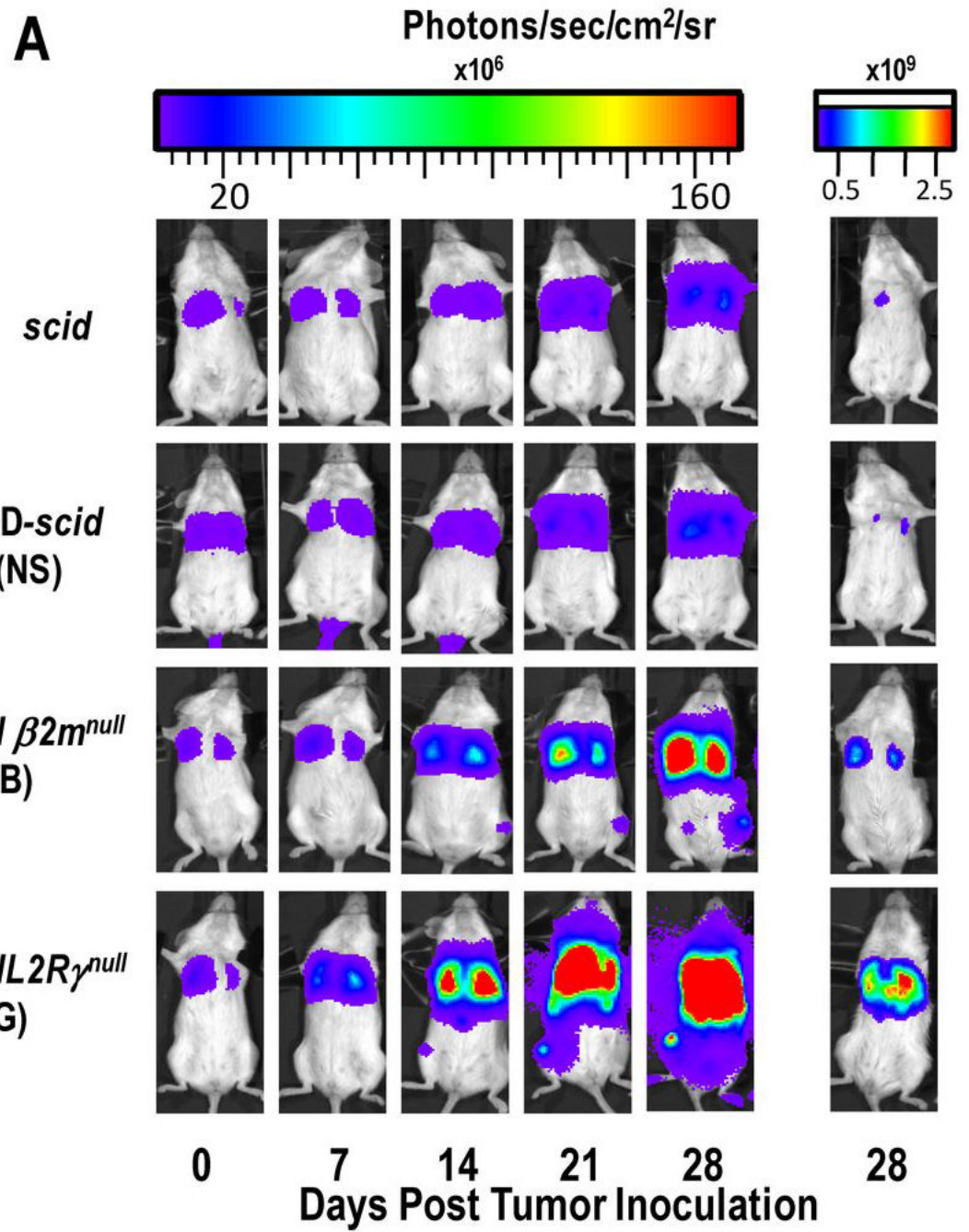
REFERENCES

1. Talmadge JE, Singh RK, Fidler IJ, Raz A. Murine models to evaluate novel and conventional therapeutic strategies for cancer. *Am J Pathol* 2007;170:793–804. [PubMed: 17322365]
2. Guy-Grand D, Azogui O, Celli S, Darce S, Nussenzweig MC, et al. Extrathymic T cell lymphopoiesis: ontogeny and contribution to gut intraepithelial lymphocytes in athymic and euthymic mice. *J Exp Med* 2003;197:333–341. [PubMed: 12566417]
3. Biron CA, Young HA, Kasaian MT. Interleukin 2-induced proliferation of murine natural killer cells in vivo. *J Exp Med* 1990;171:173–188. [PubMed: 1688606]
4. Mattern J, Bak M, Hahn EW, Volm M. Human tumor xenografts as model for drug testing. *Cancer Metastasis Rev* 1988;7:263–284. [PubMed: 3067903]
5. Giovanella BC, Vardeman DM, Williams LJ, Taylor DJ, de Ipolyi PD, Greeff PJ, et al. Heterotransplantation of human breast carcinomas in nude mice. Correlation between successful heterotransplants, poor prognosis and amplification of the HER-2/neu oncogene. *Int J Cancer* 1991;47:66–71. [PubMed: 1985881]

6. Bubenik J, Kieler J, Jandlova T, Simova J. Age-related decrease in transplantability of human tumours in nu/nu mice. *Anticancer Res* 1992;12:1695–1698. [PubMed: 1444237]
7. Marangoni E, Vincent-Salomon A, Auger N, Degeorges A, Assayag F, de Cremoux P, et al. A new model of patient tumor-derived breast cancer xenografts for preclinical assays. *Clin Cancer Res* 2007;13:3989–3998. [PubMed: 17606733]
8. Greiner DL, Hesselton RA, Shultz LD. SCID mouse models of human stem cell engraftment. *Stem Cells* 1998;16:166–177. [PubMed: 9617892]
9. Hudson WA, Li Q, Le C, Kersey JH. Xenotransplantation of human lymphoid malignancies is optimized in mice with multiple immunologic defects. *Leukemia* 1998;12:2029–2033. [PubMed: 9844934]
10. Shultz LD, Ishikawa F, Greiner DL. Humanized mice in translational biomedical research. *Nat Rev Immunol* 2007;7:118–130. [PubMed: 17259968]
11. Kim S, Poursine-Laurent J, Truscott SM, Lybarger L, Song YJ, Yang L, et al. Licensing of natural killer cells by host major histocompatibility complex class I molecules. *Nature* 2005;436:709–713. [PubMed: 16079848]
12. Shultz LD, Lyons BL, Burzenski LM, Gott B, Chen X, Chaleff S, et al. Human lymphoid and myeloid cell development in NOD/LtSz-scid IL2R gamma null mice engrafted with mobilized human hemopoietic stem cells. *J Immunol* 2005;174:6477–6489. [PubMed: 15879151]
13. Cao X, Shores EW, Hu-Li J, Anver MR, Kelsall BL, Russell SM, et al. Defective lymphoid development in mice lacking expression of the common cytokine receptor gamma chain. *Immunity* 1995;2:223–238. [PubMed: 7697543]
14. Ito M, Hiramatsu H, Kobayashi K, Suzue K, Kawahata M, Hioki K, et al. NOD/SCID/ γc^{null} mouse: an excellent recipient mouse model for engraftment of human cells. *Blood* 2002;100:3175–3182. [PubMed: 12384415]
15. Clark EA, Golub TR, Lander ES, Hynes RO. Genomic analysis of metastasis reveals an essential role for RhoC. *Nature* 2000;406:532–535. [PubMed: 10952316]
16. Hakem A, Sanchez-Sweetman O, You-Ten A, Duncan G, Wakeham A, Khokha R, et al. RhoC is dispensable for embryogenesis and tumor initiation but essential for metastasis. *Genes Dev* 2005;19:1974–1979. [PubMed: 16107613]
17. Collisson EA, De A, Suzuki H, Gambhir SS, Kolodney MS. Treatment of metastatic melanoma with an orally available inhibitor of the Ras-Raf-MAPK cascade. *Cancer Res* 2003;63:5669–5673. [PubMed: 14522881]
18. Craft N, Bruhn KW, Nguyen BD, Prins R, Liao LM, Collisson EA, et al. Bioluminescent imaging of melanoma in live mice. *J Invest Dermatol* 2005;125:159–165. [PubMed: 15982316]
19. Darrow TL, Slingluff CL Jr, Seigler HF. The role of HLA class I antigens in recognition of melanoma cells by tumor-specific cytotoxic T lymphocytes. Evidence for shared tumor antigens. *J Immunol* 1989;142:3329–3335. [PubMed: 2785141]
20. Pende D, Rivera P, Marcenaro S, Chang CC, Biassoni R, Conte R, et al. Major histocompatibility complex class I-related chain A and UL16-binding protein expression on tumor cell lines of different histotypes: analysis of tumor susceptibility to NKG2D-dependent natural killer cell cytotoxicity. *Cancer Res* 2002;62:6178–6186. [PubMed: 12414645]
21. Groh V, Bahram S, Bauer S, Herman A, Beauchamp M, Spies T. Cell stress-regulated human major histocompatibility complex class I gene expressed in gastrointestinal epithelium. *Proc Natl Acad Sci U S A* 1996;93:12445–12450. [PubMed: 8901601]
22. Groh V, Steinle A, Bauer S, Spies T. Recognition of stress-induced MHC molecules by intestinal epithelial $\gamma\delta$ T cells. *Science* 1998;279:1737–1740. [PubMed: 9497295]
23. Welte SA, Sinzger C, Lutz SZ, Singh-Jasuja H, Sampaio KL, Eknigg, et al. Selective intracellular retention of virally induced NKG2D ligands by the human cytomegalovirus UL16 glycoprotein. *Eur J Immunol* 2003;33:194–203. [PubMed: 12594848]
24. Gross S, Piwnicka-Worms D. Monitoring proteasome activity in cellulo and in living animals by bioluminescent imaging: technical considerations for design and use of genetically encoded reporters. *Methods Enzymol* 2005;399:512–530. [PubMed: 16338379]
25. Garbow JR, Zhang Z, You M. Detection of primary lung tumors in rodents by magnetic resonance imaging. *Cancer Res* 2004;64:2740–2742. [PubMed: 15087388]

26. Garbow JR, Wang M, Wang Y, Lubet RA, You M. Quantitative monitoring of adenocarcinoma development in rodents by magnetic resonance imaging. *Clin Cancer Res* 2008;14:1363–1367. [PubMed: 18316556]
27. Garbow J, Dugas J, Song S-K, Conradi M. A simple, robust hardware device for passive or active respiratory gating in MRI and MRS experiments. *Concepts in magnetic resonance, Part B: Magnetic resonance engineering* 2004;21B:40–48.
28. Ho EL, Carayannopoulos LN, Poursine-Laurent J, Kinder J, Plougastel B, Smith HR, et al. Costimulation of multiple NK cell activation receptors by NKG2D. *J Immunol* 2002;169:3667–3675. [PubMed: 12244159]
29. Carayannopoulos LN, Naidenko OV, Fremont DH, Yokoyama WM. Cutting edge: murine UL16-binding protein-like transcript 1: a newly described transcript encoding a high-affinity ligand for murine NKG2D. *J Immunol* 2002;169:4079–4083. [PubMed: 12370332]
30. Carter L, Fouser LA, Jussif J, Fitz L, Deng B, Wood CR, et al. PD-1:PD-L inhibitory pathway affects both CD4(+) and CD8(+) T cells and is overcome by IL-2. *Eur J Immunol* 2002;32:634–643. [PubMed: 11857337]
31. Gross S, Piwnica-Worms D. Spying on cancer: molecular imaging in vivo with genetically encoded reporters. *Cancer Cell* 2005;7:5–15. [PubMed: 15652745]
32. Eagle RA, Trowsdale J. Promiscuity and the single receptor: NKG2D. *Nat Rev Immunol* 2007;7:737–744. [PubMed: 17673918]
33. Diefenbach A, Jamieson AM, Liu SD, Shastri N, Raulet DH. Ligands for the murine NKG2D receptor: expression by tumor cells and activation of NK cells and macrophages. *Nat Immunol* 2000;1:119–126. [PubMed: 11248803]
34. Sutherland CL, Rabinovich B, Chalupny NJ, Brawand P, Miller R, Cosman D. ULBPs, human ligands of the NKG2D receptor, stimulate tumor immunity with enhancement by IL-15. *Blood* 2006;108:1313–1319. [PubMed: 16621962]
35. Pawelec G, Marsh SG. ESTDAB: a collection of immunologically characterised melanoma cell lines and searchable databank. *Cancer Immunol Immunother* 2005;55:623–627. [PubMed: 16421722]
36. Dorfman JR, Zerrahn J, Coles MC, Raulet DH. The basis for self-tolerance of natural killer cells in beta2-microglobulin- and TAP-1-mice. *J Immunol* 1997;159:5219–5225. [PubMed: 9548460]
37. Kollet O, Peled A, Byk T, Ben-Hur H, Greiner D, Shultz L, et al. β 2 microglobulin-deficient (β 2m^{null}) NOD/SCID mice are excellent recipients for studying human stem cell function. *Blood* 2000;95:3102–3105. [PubMed: 10807775]
38. Shultz LD, Banuelos SJ, Leif J, Appel MC, Cunningham M, Ballen K, et al. Regulation of human short-term repopulating cell (STRC) engraftment in NOD/SCID mice by host CD122+ cells. *Exp Hematol* 2003;31:551–558. [PubMed: 12829032]
39. O'Brien CA, Pollett A, Gallinger S, Dick JE. A human colon cancer cell capable of initiating tumour growth in immunodeficient mice. *Nature* 2007;445:106–110. [PubMed: 17122772]
40. Caligiuri MA. Human natural killer cells. *Blood* 2008;112:461–469. [PubMed: 18650461]
41. Gonzalez S, Groh V, Spies T. Immunobiology of human NKG2D and its ligands. *Curr Top Microbiol Immunol* 2006;298:121–138. [PubMed: 16329186]
42. Raulet DH. Roles of the NKG2D immunoreceptor and its ligands. *Nat Rev Immunol* 2003;3:781–790. [PubMed: 14523385]
43. Guerra N, Tan YX, Joncker NT, Choy A, Gallardo F, Xiong N, et al. NKG2D-deficient mice are defective in tumor surveillance in models of spontaneous malignancy. *Immunity* 2008;28:571–580. [PubMed: 18394936]
44. Zhang T, Barber A, Sentman CL. Generation of antitumor responses by genetic modification of primary human T cells with a chimeric NKG2D receptor. *Cancer Res* 2006;66:5927–5933. [PubMed: 16740733]
45. Pende D, Cantoni C, Rivera P, Vitale M, Castriconi R, Marcenaro S, et al. Role of NKG2D in tumor cell lysis mediated by human NK cells: cooperation with natural cytotoxicity receptors and capability of recognizing tumors of nonepithelial origin. *Eur J Immunol* 2001;31:1076–1086. [PubMed: 11298332]
46. Ogasawara K, Hamerman JA, Hsin H, Chikuma S, Bour-Jordan H, Chen, et al. Impairment of NK cell function by NKG2D modulation in NOD mice. *Immunity* 2003;18:41–51. [PubMed: 12530974]

47. Johansson SE, Hall H, Bjorklund J, Hoglund P. Broadly impaired NK cell function in non-obese diabetic mice is partially restored by NK cell activation in vivo and by IL-12/IL-18 in vitro. *Int Immunol* 2004;16:1–11. [PubMed: 14688055]
48. Elsner L, Muppala V, Gehrman M, Lozano J, Malzahn D, Bickeboller H, et al. The heat shock protein HSP70 promotes mouse NK cell activity against tumors that express inducible NKG2CD ligands. *J. Immunol* 2007;179:5523–5533. [PubMed: 17911639]
49. Contag CH. In vivo pathology: seeing with molecular specificity and cellular resolution in the living body. *Annu Rev Pathol* 2007;2:277–305. [PubMed: 18039101]
50. Deroose CM, De A, Loening AM, Chow PL, Ray P, Chatziioannou AF, et al. Multimodality imaging of tumor xenografts and metastases in mice with combined small-animal PET, small-animal CT, and bioluminescence imaging. *J Nucl Med* 2007;48:295–303. [PubMed: 17268028]



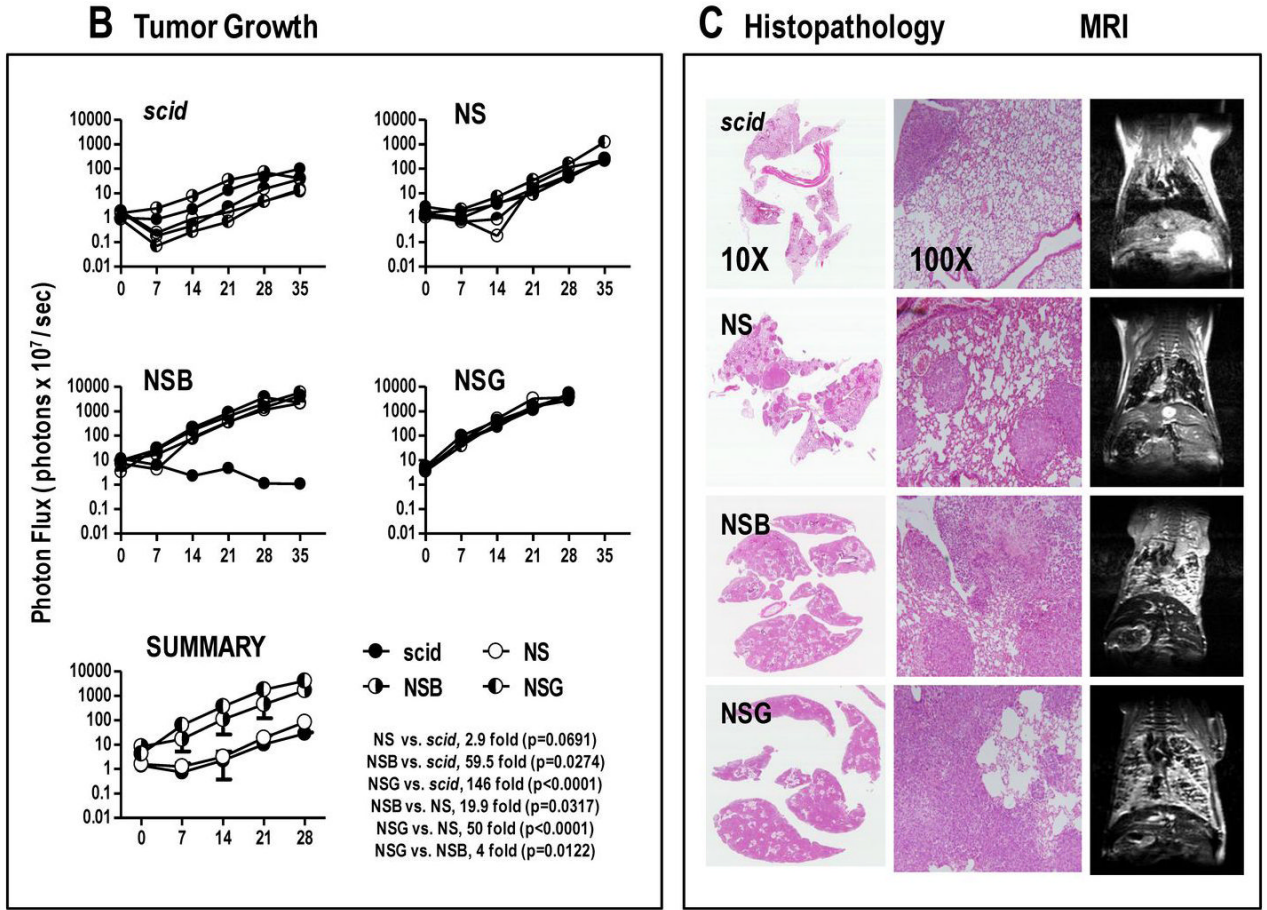


FIGURE 1. Human melanoma (A375RC-luc) engraftment in *scid*, NOD-*scid*, NOD-*scid* $\beta 2m^{null}$ and NOD-*scid* $IL2R\gamma^{null}$ mice

(A) Melanoma tumor growth was monitored by weekly bioluminescence imaging. 2.5×10^6 A375 melanoma cells expressing RhoC/luciferase (A375RC-luc) were injected intravenously and mice were imaged 2-3 h after injection (Day 0) and weekly thereafter. Weekly images from a representative mouse per strain formatted on an identical scale are shown. Reformatted images from day 28 are shown on a separate scale to demonstrate tumor confinement (bioluminescence signal) to the lungs. (B) Tumor growth was measured as photon flux (photons $\times 10^7$ /sec) at indicated times after A375RC-luc injection. A representative experiment is shown with 5 mice per group (data shown in log scale). Note that one mouse in the NSB group rejected the A375 melanoma. A summary of tumor growth (\pm SD) among strains is shown in the SUMMARY panel. On day 28, pair-wise differences in bioluminescent photon counts were statistically analyzed by the unpaired t-test. Fold mean increases between strains are indicated with respective p values. (C) Histopathology and MRI of melanoma pulmonary metastasis in immune-deficient strains. At day 28 (NSG) or day 35 (all other strains) tumor growth was monitored by MRI imaging. Representative slides at 10x and 100x magnifications are shown. Mean tumor burden is estimated as percentage of total lung parenchyma; tumor burden in each strain (average of two mice) is: *scid*, 7%; NS, 35%; NSB, 62%, and NSG, 95%. One representative MRI coronal image per mouse per strain is shown.

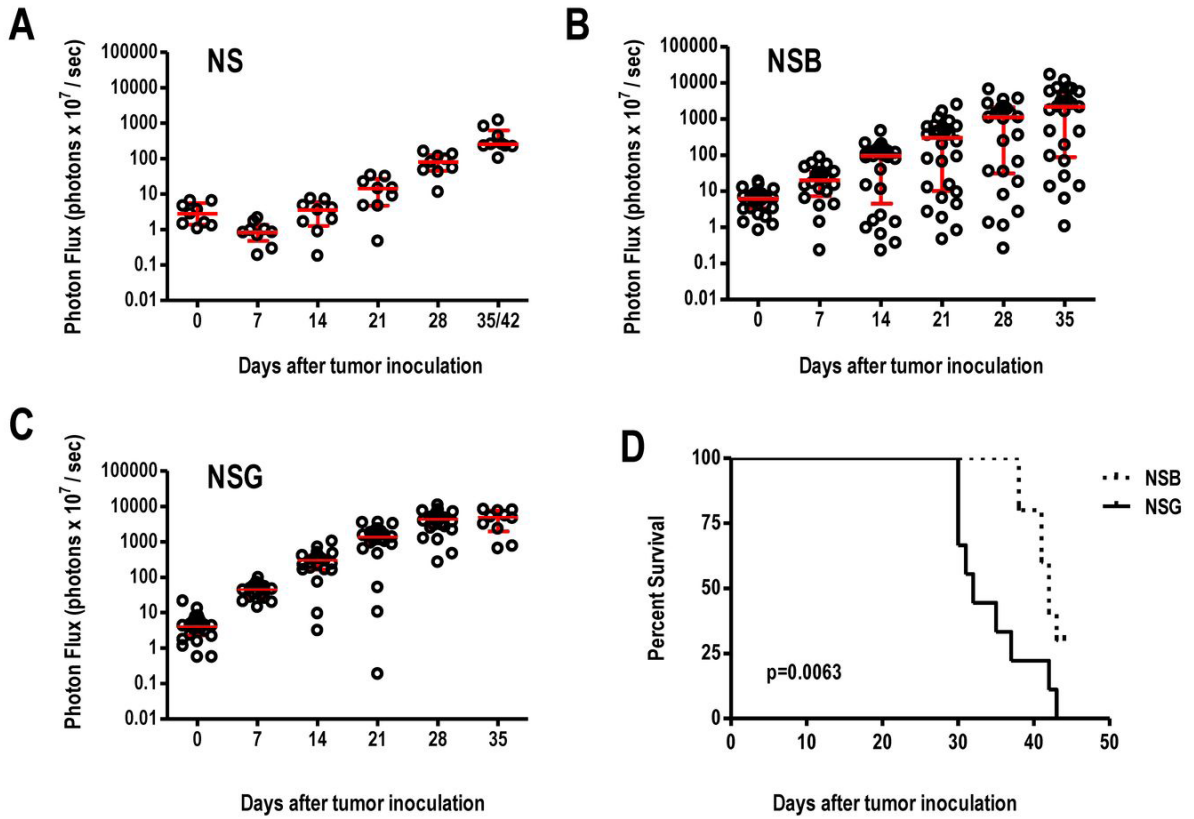


FIGURE 2. Tumor growth and survival in NOD-*scid*, NOD-*scid* $\beta 2m^{\text{null}}$, and NOD-*scid* *IL2R γ ^{null}* mice

Tumor growth was monitored by bioluminescence imaging: (A) NS (n=14), (B) NSB (n=28) and (C) NSG (n=32). Summary scatter dot plots with each dot representing one mouse are shown. Data represents 4 independent experiments. The horizontal red line indicates the median value and top-bottom of the whiskers plot represent 75% and 25% percentile, respectively. (D) Survival curve of tumor-bearing NOD-*scid* $\beta 2m^{\text{null}}$ and NOD-*scid* *IL2R γ ^{null}* mice. Mice were injected intravenously with 2.5×10^6 A375RC-luc cells and monitored weekly by BLI (n=10 mice per strain). Mice were sacrificed if weight dropped below 20% of initial. Curves were compared using the Log-rank test. One of three independent experiments is shown.

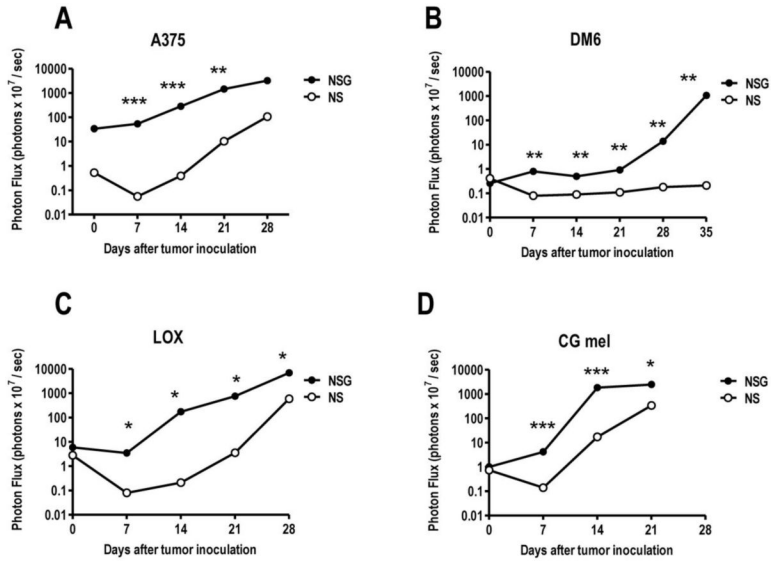


FIGURE 3. NOD-scid *IL2R γ* ^{null} mice are permissive for growth of multiple melanoma lines NS or NSG were injected intravenously with 2.5×10^6 (A) A375, (B) DM6, (C) Lox or (D) CG mel (a primary melanoma cell line) expressing RhoC/luciferase; tumor growth was monitored by weekly bioluminescence. Average photon flux is shown (n=3 mice/strain/line). In all instances, melanoma pulmonary metastases grew faster in the NSG mice. Pair-wise differences in bioluminescent photon counts were statistically analyzed by the unpaired t-test at each time point, p values are shown: * p<0.05; ** p<0.005; *** p<0.0005.

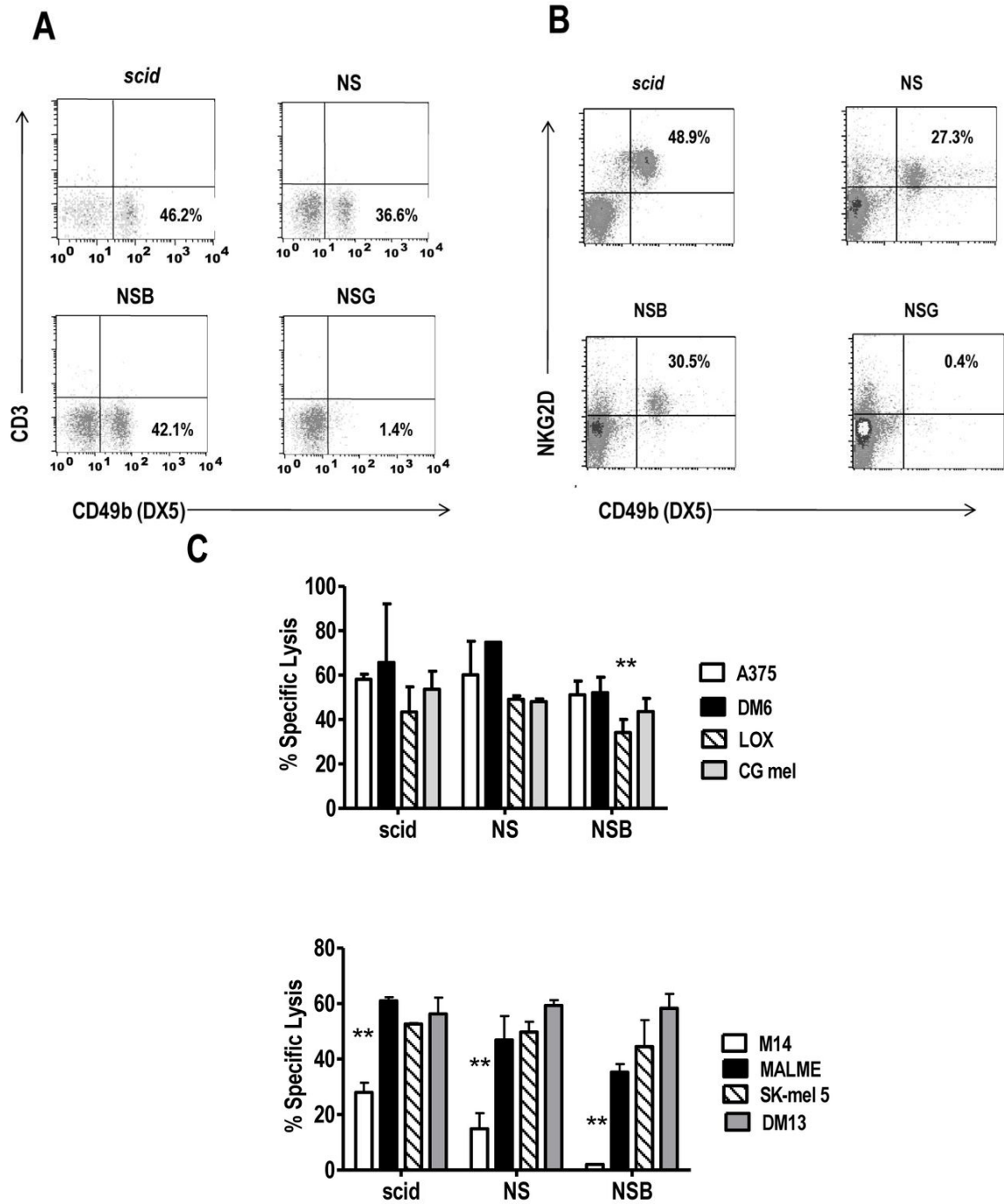


FIGURE 4. NK cell populations in *scid*, *NOD-scid*, *NOD-scid* $\beta 2m^{null}$ mouse strains display *in vitro* cytotoxicity against human melanoma cell lines

Spleen cell suspensions were stained with (A) anti-CD45.1, anti-CD3 and anti-pan NK cell (DX5) antibodies or (B) anti-CD45.1, anti-pan NK cell (DX5) and anti- NKG2D antibodies. Percentages are reported based on CD45.1+ gated cells; within the whole spleen cell population (CD45.1+ and CD45.1-), DX5/NKG2D double positive cells are 12.6%, 8.8% and 9.3% in *scid*, NS and NSB, respectively. In NSG spleen cells, no reactivity was observed with DX5 antibody and anti-NKG2D mAb confirming the absence of NK cells in NSG. A representative mouse (n=5) is shown. (C) IL-15 + IL-18 activated NK cells from *scid*, *NOD-scid*, *NOD-scid*

$\beta 2m^{null}$ display cytotoxic activity against human melanoma lines. Spleen cells (2×10^6 cells/ml) were activated with IL-15 (100 ng/ml) and IL-18 (100 ng/ml) for 48 h, harvested and used as effectors in a 4 h ^{51}Cr -release assay. IL-15 + IL-18 treated NOD-*scid* $IL2R\gamma^{null}$ spleen cells did not yield any viable cells. In the experiment shown, the E:T ratio is 30:1. YAC targets were used as the positive control (data not shown). Data is representative of four independent experiments. Lysis of melanoma cell lines by each mouse strain was analyzed by repeated measure one way ANOVA followed by Tukey's analysis. **, p values <0.005 are statistically significant.

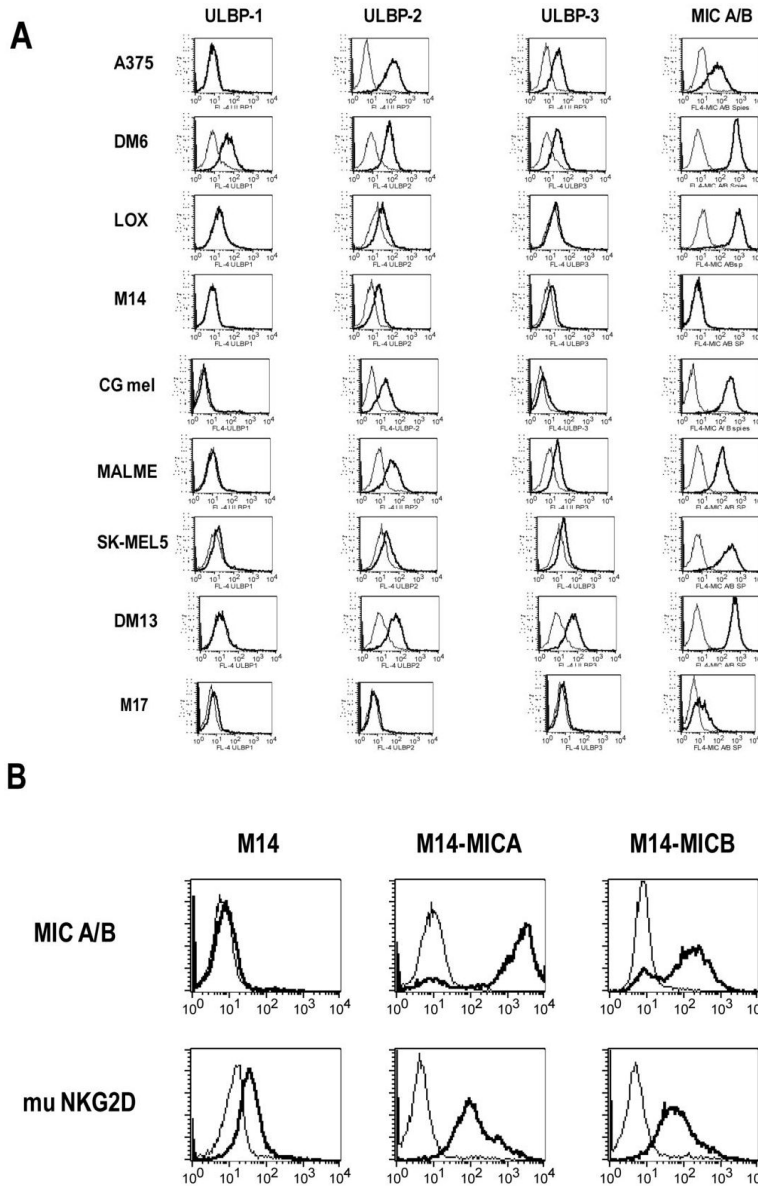


FIGURE 5. Expression of NKG2D ligands, MICA/B and ULBP 1-3, by human melanoma cell lines (A) Melanoma cell lines were stained using anti-ULBPs and the 6D4 anti-MICA/B mAbs and analyzed by flow cytometry. ULBPs and MICA/B expression (thick line) and the isotype control (thin line) are shown in each histogram. Data is representative of 3 independent experiments. (B) M14, M14-MICA and M14-MICB cells were stained with (top panel) anti-MICA/B 6D4 (thick line), isotype control (thin line) or (bottom panel) murine NKG2D tetramer (thick line) or control tetramer (thin line). Data is representative of 2 independent experiments.

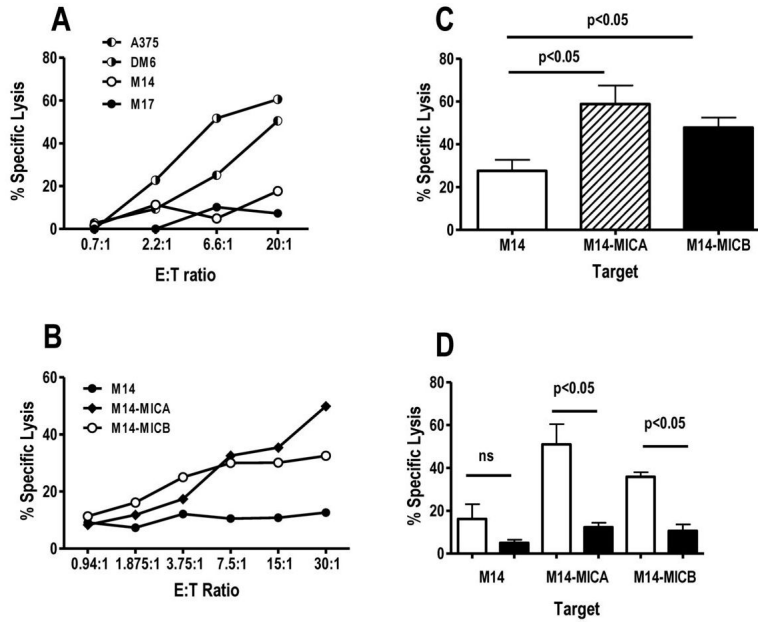


FIGURE 6. Human melanoma recognition by NOD-*scid* NK cells correlates with MICA/B expression and is blocked by anti-murine NKG2D antibody
 (A) NS spleen cells were activated with IL-15 + IL-18 for 48 h, harvested and incubated with ⁵¹Cr-labeled targets for 4 h as described in Materials and Methods (n=3 experiments). MICA/B expression by M14, M17, A375 and DM6 is shown in Figure 5. (B) NS NK cells were tested at the indicated E:T ratios in ⁵¹Cr-release assay using M14, M14-MICA and M14-MIB transfectants (n=3 experiments) (C) Recognition of M14-MICA and M14-MICB transfectants by NK cells from NS mice. The mean value (+/- 1SD) at a 30:1 E:T ratio is shown from six independent experiments. The lower killing of M14-MICB (compared to MICA) likely reflects the lower antigen expression level on the M14-MICB target cell population. (D) Recognition of M14-MICA and M14-MICB by NS NK cells is blocked by anti-murine NKG2D mAb. NS spleen cells were cultured in IL-15 + IL-18 for 48 h, harvested and incubated with anti-muNKG2D mAb (black bars) or isotype control (white bars) for 1 h (30 ug/ml), ⁵¹Cr-labeled target cells added and assay performed as described in Materials and Methods. E:T ratio is 30:1 (n=3 experiments). Data in (C) and (D) was analyzed by repeated measure one way ANOVA followed by Tukey's analysis. P values <0.05 are statistically significant.